

PERFORMANCE EVALUATION OF MOLYBDENUM BLADES IN AN X-RAY PINHOLE CAMERA

L.M. Bobb, A.F.D. Morgan, G. Rehm, Diamond Light Source, Oxfordshire, U.K.

Abstract

At Diamond Light Source transverse profile measurements of the 3 GeV electron beam are provided by x-ray pinhole cameras. From these beam size measurements and given knowledge of the lattice parameters the emittance, coupling and energy spread are calculated. Traditionally, tungsten blades are used to form the pinhole aperture due to the opacity of tungsten to x-rays in the keV spectral range. The physical properties of tungsten also make it difficult to work. To achieve the $25 \mu\text{m} \times 25 \mu\text{m}$ aperture size required for high resolution measurements it is necessary to mount these tungsten blades in an assembly whereby the pinhole aperture size is defined by precisely machined shims. Here we propose to replace the tungsten blade and shim arrangement with machined molybdenum blades and evaluate the performance of the resulting imaging system.

INTRODUCTION

In order to provide high brilliance x-rays for user experiments, third generation synchrotron radiation facilities must operate with low vertical emittance beams. The emittance of the electron beam is derived from measurements of the transverse beam profile [1, 2] and may be controlled via a feedback system [3]. This necessitates the need for high resolution, robust and online beam size monitoring.

There are various non-invasive techniques to measure the transverse beam profile using synchrotron radiation in the visible to x-ray spectral range [4–7]. In this paper we focus on the use of x-ray pinhole cameras.

Currently there are two pinhole cameras in the vertical emittance feedback system which are referred to as “pinhole 1” and “2” respectively. The layout of these pinhole cameras is shown in Fig. 1. Two different bending magnet locations provide synchrotron radiation to each of the pinhole cameras. The synchrotron radiation is passed from the storage ring vacuum to air through a 1 mm thick aluminium window. Due to the spectral transmission of aluminium the transmitted beam is filtered. The beam is filtered further by its transmission through air from the window to the pinhole and from the pinhole to the PreLude 420 scintillator screen. The source has a spectrum from approximately 15 keV to above 60 keV [1]. To prevent oxide growth the pinhole assemblies are kept under nitrogen.

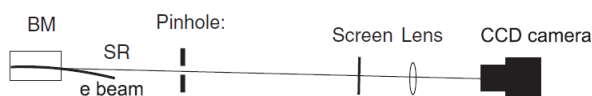


Figure 1: Schematic of the pinhole camera system [1].

The pinhole assembly arrangement of pinhole systems 1 and 2 are identical. The pinhole apertures are formed by stacking two orthogonal sets of (25 mm(h) × 1 mm(v) × 5 mm(d)) tungsten blades separated by precisely machined shims. The thickness of the shims between the tungsten blades sets the aperture size e.g. to form a $25 \mu\text{m}$ aperture a pair of $25 \mu\text{m}$ thick shims are positioned between the ends of a pair of tungsten blades.

The spatial resolution of an imaging system may be described by the point spread function (PSF). The PSF is assumed to be constant on relatively long timescales for a given imaging system and is approximated by a Gaussian distribution of standard deviation σ_{PSF} . For a pinhole camera imaging system the overall PSF may be represented as

$$\sigma_{PSF}^2 = \sigma_{pinhole}^2 + \sigma_{camera}^2 \quad (1)$$

with

$$\sigma_{pinhole}^2 = \sigma_{diffraction}^2 + \sigma_{aperture}^2 \quad (2)$$

and

$$\sigma_{camera}^2 = \sigma_{screen}^2 + \sigma_{lens}^2 + \sigma_{CCD}^2 \quad (3)$$

where the subscripts denote the sources of the PSF contributions. The PSF contribution associated with imaging the scintillator screen denoted σ_{camera} may be measured using a knife-edge. The PSF contribution from the pinhole denoted $\sigma_{pinhole}$ may be calculated given the aperture size is known [1].

Due to the tungsten and shim arrangement, although the thickness of the shim is known, the absolute effective aperture size available to pass beam is not well defined. The

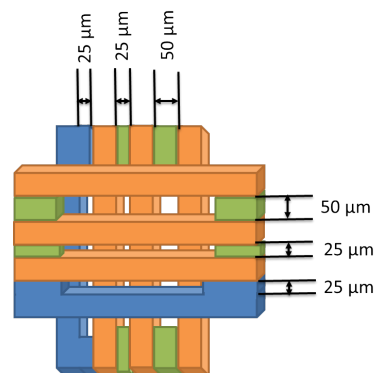


Figure 2: A schematic of the downstream view of the pinhole 3 assembly showing the arrangement of the machined molybdenum blades (blue), tungsten blades (orange) and shims (green).

effective aperture size depends on the shim thickness, the shim positioning, the amount of burring from cutting the shims to fit in the pinhole assembly, the pressure applied to the tungsten stack once mounted in the holder and the orientation angle of the pinhole assembly relative to the synchrotron radiation beam.

A third pinhole system referred to as “pinhole 3” has been installed for research and development to improve the design and operation of the x-ray pinhole cameras used for vertical emittance feedback. Pinhole 3 is nominally identical to the pinhole 2 imaging system.

To reduce the number of degrees of freedom of the pinhole assembly, the tungsten and shim arrangement could be replaced by machined molybdenum blades. In this case the aperture size is defined by the machined depth in the molybdenum blade. The pinhole assembly under test in the pinhole 3 system features $25\ \mu\text{m} \times 25\ \mu\text{m}$ apertures formed using molybdenum blades and tungsten blades with shims as shown in Fig. 2. This arrangement allows a direct comparison to be made between the two aperture designs.

COMPARISON OF PINHOLE ANGLE SCANS

The pinhole assembly is mounted on translation and rotation mechanisms to allow for remote alignment with the synchrotron radiation beam. Horizontal and vertical angle scans were performed for the $25\ \mu\text{m} \times 25\ \mu\text{m}$ molybdenum and tungsten apertures of pinhole system 3.

During each scan, a 2D Gaussian was fitted to each image and the horizontal and vertical beamsizes $\sigma_{x,y}$, peak intensity and fit error were recorded. These parameters were then normalised relative to their maximum or minimum value and plotted as a function of rotation angle. In Figures 3 and 4 the horizontal and vertical angle scans are shown respectively for the molybdenum (dashed lines) and tungsten (solid lines) apertures.

In both the horizontal and vertical scans, from a rotation angle of -0.175 deg the peak intensity is expected to increase linearly reaching a maximum at 0 deg and be symmetric about the 0 deg position. Due to the length of the pinhole assembly along the beam path, it is appropriate to consider the pinhole aperture as a three dimensional tunnel rather than a two dimensional screen. Therefore it is expected that the maximum peak intensity should be recorded when the pinhole assembly is aligned in parallel with the incident beam.

In Figures 3 and 4 the peak intensity of the tungsten aperture shows the expected behaviour whereas the molybdenum aperture exhibits a non-linear distribution with strong asymmetry. Referring to the bottom left aperture of Fig. 2, the observed asymmetry may be explained by the blade arrangement of the pinhole assembly. Within each stack, the molybdenum aperture has a molybdenum blade on one side and a tungsten blade on the other. The non-linear dependence of the measured peak intensity must be related to the transmission of x-rays in molybdenum and could indicate

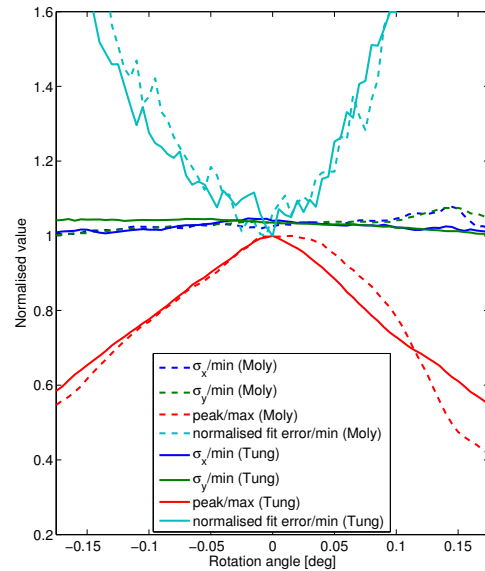


Figure 3: Horizontal rotation scans on pinhole camera 3 of the molybdenum aperture (dashed lines) and tungsten aperture (solid lines).

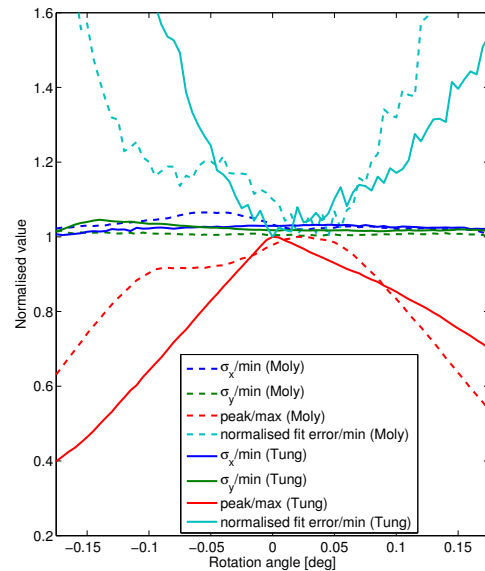


Figure 4: Vertical rotation scans on pinhole camera 3 of the molybdenum aperture (dashed lines) and tungsten aperture (solid lines).

oxide or nitride growth on the molybdenum blades. This behaviour is more strongly shown in the vertical scan than the horizontal scan.

The measured transverse beam sizes and fit errors as a function of rotation angle in the horizontal and vertical directions are not seen to strongly differ between the molybdenum and tungsten apertures.

PSF MEASUREMENT USING THE TOUSCHEK LIFETIME

Coulomb scattering of charged particles in a stored beam causes an exchange of energies between the transverse and longitudinal motion. The Touschek effect is the transformation of a small transverse momentum into a large longitudinal momentum due to scattering. In this single scattering event, both of the particles are lost since one particle has too much energy and the other has too little [8].

The loss of particles due to the Touschek effect may considerably reduce the beam lifetime in storage rings. The Touschek lifetime T_ℓ for the ultrarelativistic case is defined as

$$\frac{1}{T_\ell} \approx \left\langle \frac{cr_p^2 N_p}{2\sqrt{\pi}\gamma^2 \sigma_s \sqrt{\sigma_x^2 \sigma_y^2 - \sigma_p^4 D_x^2 D_y^2 \delta_m^2}} \right\rangle, \quad (4)$$

where r_p is the classical particle radius, c is the speed of light, N_p is the number of particles in the bunch, γ is the Lorentz factor, σ_s is the bunch length, $\sigma_{x,y}$ are the horizontal and vertical beam sizes, σ_p is the relative momentum spread, $D_{x,y}$ are the horizontal and vertical dispersions and δ_m is relative momentum spread. The brackets denote the average over the whole circumference of the storage ring [8].

In the case of a plane orbit and without coupling of the horizontal dispersion [8, 9], the vertical dispersion D_y is zero and Eq. (4) reduces to

$$\frac{1}{T_\ell} \approx \left\langle \frac{cr_p^2 N_p}{2\sqrt{\pi}\gamma^2 \sigma_s \sigma_x \sigma_y \delta_m^2} \right\rangle. \quad (5)$$

Assuming all other parameters remain constant, the Touschek lifetime size is directly proportional to the vertical beam size. To ensure the simplification to the plane orbit case is appropriate, the term in the root of the denominator $\sigma_x^2 \sigma_y^2 - \sigma_p^4 D_x^2 D_y^2$ was compared when D_y is zero and when D_y is set to the real value of 4.54×10^{-3} m. Values have been taken from measurements on pinhole camera 2: σ_x is $43.3 \mu\text{m}$, σ_y is $15.8 \mu\text{m}$, σ_p is 1.1×10^{-3} , D_x is 2.23×10^{-2} m and D_y is 4.54×10^{-3} m. It is found that with the plane orbit approximation this denomination term is increased by 3.3% which is within the measurement error.

The images acquired from the pinhole camera are fitted with a 2D Gaussian distribution. Considering the vertical beam size only, it is known that the measured beam size will be larger than the true beam size due to the PSF. Therefore the measured beam size σ_M is given by

$$\sigma_M = \sqrt{\sigma_y^2 + \sigma_{PSF}^2}. \quad (6)$$

From Eq. (6) it is seen that when $\sigma_y \gg \sigma_{PSF}$ such that the PSF is negligible then the measured beam size is equal to the true beam size i.e. $\sigma_M = \sigma_y$. The effect of the PSF contribution to the measurement increases as the true beam size is reduced. In order to obtain the true beam size σ_y from the measurement, the PSF spread value σ_{PSF} must be known.

With the 400 bunch and 200 mA beam current the measured beam lifetime τ is Touschek dominated such that $\tau \approx T_\ell$. In the Touschek dominated regime the measured beam lifetime is used as a proxy measurement for the true beam size as

$$\sigma_y = k\tau, \quad (7)$$

where k is a scaling factor. Substituting Eq. (7) into Eq. (6) the measured beam size is

$$\sigma_M = \sqrt{(k\tau)^2 + \sigma_{PSF}^2}. \quad (8)$$

The 2D Gaussian fitter outputs the beam size σ_y by removing the PSF contribution from the measured beam size using Eq. (6). In order to obtain the measured beam size σ_M from the fitter, the PSF value σ_{PSF} is set to zero.

With the Touschek dominated beam and starting from a large vertical beam size, using the skew quads the vertical beam size was gradually reduced. For each skew quad setting the beam lifetime τ , current and measured beam size σ_M were recorded.

In Fig. 5 the measured beam size versus beam conditioning number is shown for pinholes 1, 2 and the molybdenum aperture of pinhole system 3. The beam conditioning number is the product of beam lifetime and current. At large beam sizes a linear regime is observed in Fig. 5. This is expected since the PSF is negligible in comparison to be the beam size such that $\sigma_M = k\tau$. As the beam size becomes comparable to the PSF, at approximately 1250 mA h in Fig. 5, the data is no longer linear and the PSF cannot be ignored.

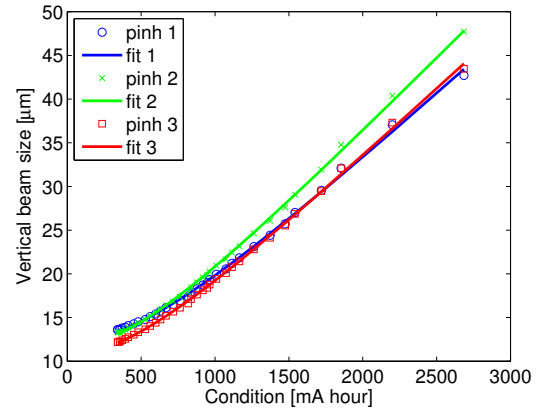


Figure 5: A plot of the measured vertical beam size against beam conditioning number for pinhole systems 1, 2 (measurement 1) and the molybdenum aperture of pinhole system 3.

Each dataset has been fitted using the method of least squares with Eq. (8) to obtain the scaling parameter k and PSF σ_{PSF} for each pinhole imaging system. The fit results are shown in Table 1. The scaling factor is expected to be constant given the assumption of Eq. (7). The average scaling factor from Table 1 is $(1.57 \pm 0.09) \times 10^{-2} \mu\text{m mA}^{-1} \text{h}^{-1}$.

Table 1: Fit Results of the Scaling Factor and PSF from Figures 5 and 6

Pinhole camera	Measurement 1		Measurement 2	
	k [$\mu\text{m mA}^{-1} \text{h}^{-1}$]	σ_{PSF} [μm]	k [$\mu\text{m mA}^{-1} \text{h}^{-1}$]	σ_{PSF} [μm]
1	0.0155	12.36	0.0143	12.33
2	0.0173	11.67	0.0160	11.70
3	Molybdenum		Tungsten	
	k [$\mu\text{m mA}^{-1} \text{h}^{-1}$]	σ_{PSF} [μm]	k [$\mu\text{m mA}^{-1} \text{h}^{-1}$]	σ_{PSF} [μm]
	0.0159	10.82	0.0152	16.28

In Fig. 6 the measured beam size versus beam conditioning number is shown for pinholes 1, 2 and the tungsten aperture of pinhole system 3. The fit results are shown in Table 1. Comparing the PSF values from Table 1 of pinhole cameras 1 and 2, there is a difference of $0.03 \mu\text{m}$ between the repeated measurements showing a good level of repeatability. The mean PSF values for pinhole cameras 1 and 2 are $12.35 \mu\text{m}$ and $11.68 \mu\text{m}$ respectively. The repeated PSF measurement for pinholes 1 and 2 should be consistent since no changes were made to these imaging systems.

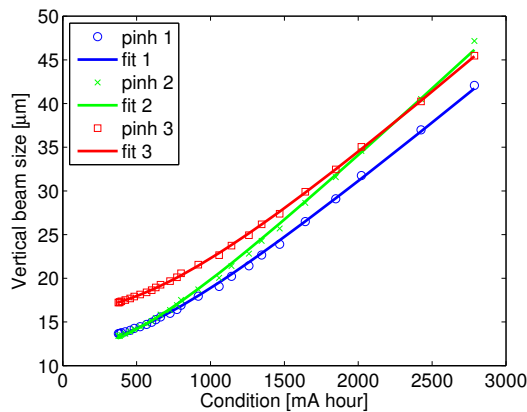


Figure 6: A plot of the measured vertical beam size against beam conditioning number for pinhole systems 1, 2 (measurement 2) and the tungsten aperture of pinhole system 3.

The PSF measurements from the molybdenum and tungsten apertures of the pinhole 3 system show a difference of $5.46 \mu\text{m}$. From visual inspection the tungsten aperture is approximately double the size of the molybdenum aperture. The PSF measurement on pinhole 3 is larger than that of pinhole system 2. Since these systems are nominally the same it is likely that the tungsten aperture on pinhole 3 is also larger than that on pinhole 2.

Given that the pinhole systems 2 and 3 are nominally identical, the PSF value of the tungsten aperture on pinhole 2 may be compared with the molybdenum aperture on pinhole 3. In Table 1, the molybdenum aperture has a PSF value which is $0.85 \mu\text{m}$ smaller than the tungsten aperture indicating that the aperture size using the simpler molybdenum setup is closer to the specification value of $25 \mu\text{m}$.

CONCLUSION

Angle scans of the pinhole assembly relative to the incident synchrotron radiation beam have been performed to study the opacity of molybdenum to keV x-rays. Results show that although the peak intensity as a function of angle for the molybdenum aperture is somewhat non-linear in comparison to tungsten, this has a negligible affect on the beam size measurement.

PSF measurements of each pinhole imaging system were acquired using the Touschek lifetime with a good level of repeatability. By replacing the tungsten and shim assembly with machined molybdenum blades, the numerous of degrees of freedom which affect the aperture size in the pinhole system were removed such that the PSF was reduced.

REFERENCES

- [1] C. Thomas et al., “X-ray pinhole camera resolution and emittance measurement”, Phys. Rev. ST Accel. Beams 13, 022805, (2010).
- [2] A. Andersson et al., “Determination of a small vertical electron beam profile and emittance at the Swiss Light Source”, Nucl. Instrum. Meth. A591, (2008), 437–446.
- [3] I.P.S. Martin et al., “Operating the Diamond Storage Ring with Reduced Vertical Emittance”, Proc. of IPAC2013, Shanghai, China, MOPEA071.
- [4] J. Breunlin et al., “Methods for measuring sub-pm rad vertical emittance at the Swiss Light Source”, Nucl. Instrum. Meth. A803, (2015), 55–64.
- [5] P. Elleaume et al., “Measuring Beam Sizes and Ultra-Small Electron Emittances Using an X-ray Pinhole Camera”, J. Synchrotron Rad., (1995). 2, 209-214.
- [6] T. Mitsuhashi, “Measurement of small transverse Beam Size Using Interferometry”, Proc. of DIPAC 2001, ESRF, Grenoble, France, IT06.
- [7] K. Iida et al., “Measurement of an electron-beam size with a beam profile monitor using Fresnel zone plates”, Nucl. Instrum. Meth. A506, (2003), 41–49.
- [8] A. Piwinski, “The Touschek effect in strong focusing storage rings”, DESY 98-179, 1998, <http://arxiv.org/abs/physics/9903034>.
- [9] R. Dowd et al., “Achievement of ultralow emittance coupling in the Australian Synchrotron storage ring”, Phys. Rev. ST Accel. Beams 14, 012804 (2011).